NANO LETTERS

pubs.acs.org/NanoLett

Letter

Prediction of a Novel Electromechanical Response in Polar Polymers with Rigid Backbones: Contrasting Furan-Derived Nanothreads to Poly(Vinylidene Fluoride)

Tao Wang, Yawei Gao, Bo Chen, Vincent H. Crespi, and Adri C. T. van Duin*

Cite This: *Nano Lett.* 2024, 24, 9195−9201

Read Online

ACCESS | Metrics & More | Article Recommendations | Supporting Information

ABSTRACT: *Syn* furan nanothreads have all oxygen atoms arranged on one side of the thread backbone; these polar threads present intriguing opportunities in electromechanical response owing to their rigid ladder-like backbone. We retrained a C/H/O reactive force field to simulate their response to external electric field for both end-anchored individual threads and bulk nanothread crystals, contrasting the results to those for poly(vinylidene fluoride) (PVDF) polymer. Whereas the field induces a length-independent torque in PVDF through backbone rotation about σ bonds, furan-derived nanothreads generate a length-dependent torque by progressively twisting their rigid backbone. This mode of response couples the *rotational history* of the electric field to axial tension in the anchored thread. In simulations of densely packed *syn* furan nanothread crystals without anchors, the crystals pole in a field (∼3 GV/m at 300 K) similar to that seen in simulations of PVDF, suggesting that crystals of polar nanothreads can be ferroelectric.

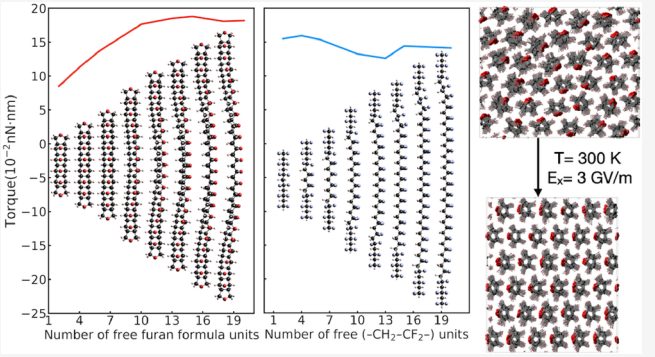

KEYWORDS: *furan nanothreads, PVDF, ReaxFF, ferroelectricity, nanoelectromechanics*

Carbon nanothreads are one-dimensional sp^3-rich nanomaterials[1−4] with very narrow cross sections, thinner even than carbon nanotubes.[5] They promise high tensile strength and rigidity[6] compared to traditional polymers, with similar chemical tunability. These materials were first synthesized through uniaxial polymerization in molecular crystals of benzene induced by slow compression/decompression at room temperature.[1] This method was later applied to a broad range of precursors such as pyridine,[7] thiophene,[8] cubane,[9] naphthalene/octafuoronaphthalene cocrystals,[10] Ar−OH/ArF−OH cocrystals,[11,12] and others.[13−16] The onset of polymerization is typically >15 GPa, but this is reduced to ∼10 GPa when using a less aromatic precursor such as furan, facilitating the scaling of synthesis volumes.[17,18] Furan-derived nanothreads in the *syn* structure of Figure 1 array the oxygen atoms along one side of the backbone, thus producing a transverse dipole moment that suggests a potential for novel modes of electromechanical response possibly enriched by the thread's relatively stiff backbone and the steric repulsion between neighboring oxygens along the thread axis.[19] Recently, furan *syn* nanothreads functionalized with carboxyl groups have been synthesized by compressing 2,5-furandicarboxylic acid,[20,21] which aligns with predictions that the *syn* allotrope may be stabilizable through precursor functionalization.[22]

In contrast to ladder-like furan nanothreads, the well-known organic ferroelectric polymer poly(vinylidene fluoride) (PVDF) connects its $-CH_2-$ and $-CF_2-$ subunits with individual σ bonds; thus, it is much more flexible. PVDF has three known conformations, TGTG′, TTTT, and TTTGTTTG′, with different arrangements of $-CH_2-$ and $-CF_2-$ units along the backbone (T: *trans*, G: *gauche*$^+$, G′: *gauche*$^-$). These various conformations can crystallize into α, β, γ, and δ phases (Figure S1). The most stable phase, α, has the TGTG′ conformation, as shown in Figure 1. The β phase has remarkable piezo-, pyro-, and ferro-electric properties due to its all-T planar zigzag conformation and a parallel arrangement of the two chains in a unit cell.[23] The β phase can be promoted from the α phase (or other configurations) by an external electric field or mechanical deformation.[24]

Here we seek novel modes of electromechanical response that may arise from the exceptional torsional rigidity of nanothreads. To this end, we contrast the electric field response of furan *syn* nanothreads to that of PVDF oligomers in two distinct situations: (1) the idealized geometry of a single

Received: March 25, 2024
Revised: July 10, 2024
Accepted: July 11, 2024
Published: July 17, 2024

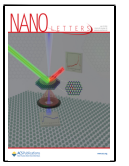

https://doi.org/10.1021/acs.nanolett.4c01431
Nano Lett. 2024, 24, 9195−9201

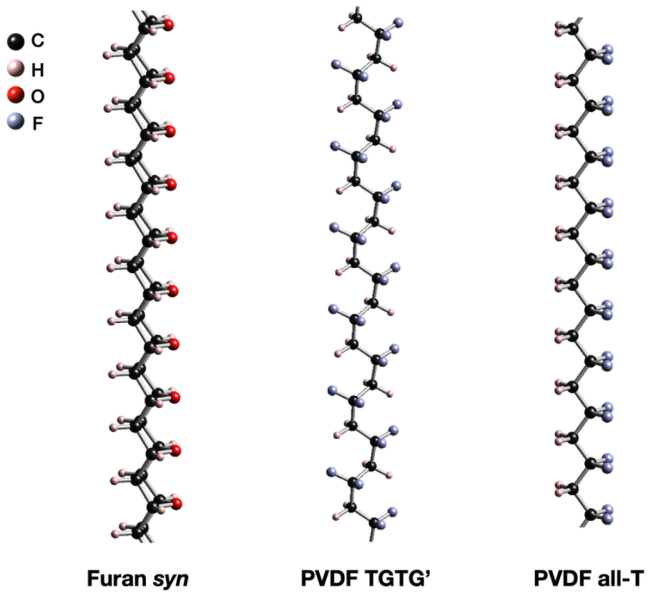

Figure 1. *Syn* furan nanothread and PVDF as TGTG′ or TTTT ("all-T") chains.

chain (nanothread or all-T PVDF) anchored on both ends to interrogate torque transmission down the polymer backbone, and (2) a dense packing of furan *syn* nanothreads or PVDF chains to study collective effects during chain reorientation. We retrained the parameters of a previous C/H/O ReaxFF reactive force field[25] for the furan *syn* thread systems and used the C/H/O/F/Al ReaxFF Force Field of Gao et al.[26] (included in Supporting Information) for the PVDF systems. The PVDF force field showed excellent agreement with both density functional theory (DFT) calculations and experimental measurements in terms of the PVDF polarizability, single chain stability, and crystalline phase stability.[26]

Reactive Force Field Optimization and Validation. To describe furan threads, we fine-tuned the ReaxFF reactive force field parameters developed by Chenoweth et al.[25] for combustion in C/H/O systems (hereafter called ReaxFF$_{CHO2008}$) to more accurately describe the atomic charges and stiffness of furan-derived nanothreads. ReaxFF$_{CHO2008}$ overestimates the Diels-Alder transition barrier for furan dimerization (Figure S2) and underestimates the bending stiffness of furan *syn* thread oligomers (Figure 2). We retrained this force field against first-principles density functional results for the energy difference between straight and bent oligomers and optimized the atomic charges against first-principles Bader charges for *syn* furan threads (Table S1). Isolated furan thread oligomers tend to bend to reduce the repulsive interactions between successive oxygen atoms. ReaxFF$_{furan2024}$ reproduces the energy difference between straight and bent furan oligomers (calculated in DFT) significantly better than does ReaxFF$_{CHO2008}$, as shown in Figure 2. The transverse dipole moment of furan *syn* threads obtained from DFT using the Berry phase method is 0.26 eÅ per furan formula unit; that from the ReaxFF$_{furan2024}$ is very similar, 0.27 eÅ (the dipole moment obtained with ReaxFF$_{CHO2008}$ is not so different, 0.25 eÅ per furan formula unit). The ability of ReaxFF$_{furan2024}$ to describe both the backbone stiffness and the dipolar character of the furan-derived thread suggests that it is suitable for an investigation of the electromechanical response.

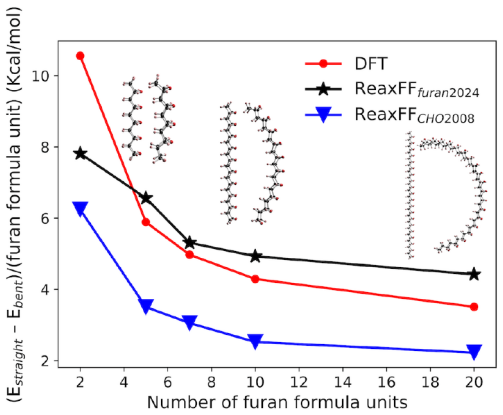

Figure 2. Energy difference per furan formula unit between straight and bent furan *syn* thread oligomers from DFT, ReaxFF$_{CHO2008}$, and ReaxFF$_{furan2024}$.

We also discovered that the optimized potential better reproduces the activation barrier to furan dimerization, reducing the discrepancy against density functional results from 12.3 kcal/mol with ReaxFF$_{CHO2008}$ to 4.9 kcal/mol with ReaxFF$_{furan2024}$ (Figure S2). Supporting Information provides further details on this new reactive potential.

Molecular Dynamics. To simulate the response to an external electric field, we performed molecular dynamics (MD) simulations using ReaxFF$_{furan2024}$ and ReaxFF$_{PVDF}$ from Gao et al.[26] The simulations used the velocity Verlet algorithm[27] within the standalone ReaxFF code to investigate the electromechanical response of anchored furan *syn* thread oligomers and PVDF all-T chain oligomers. The Nose–Hoover thermostat implemented in LAMMPS[28] was employed to simulate the poling of randomly packed furan *syn* threads and PVDF crystal. A time step of 0.25 fs was applied to both simulations. For the bulk systems, we packed 36 furan *syn* threads and PVDF TGTG′ chains with a random distribution of azimuthal orientations and axial shifts in 6 × 6 supercells with periodic boundary conditions. Each furan *syn* thread or PVDF TGTG′ chain has 60 furan formula (C_4H_4O) units or 12 ($-CH_2-CF_2-$) units, respectively. Longer simulation cells provide a more accurate treatment of rotational barriers under nonconcerted rotations. More details about the MD simulations are included in SI Sections 3 and 4.

Torque Induced in the Backbone of an Isolated *Syn* Nanothread or All-T PVDF Chain by an External Electric Field. When under an electric field that is not aligned with their intrinsic permanent dipole moments, polar polymers reorient these moments through molecular rotation or local bond distortions to better align with the field. Ramos et al.[29] reported that a free or end-anchored all-T PVDF chain undergoes significant rotation, bending, and bond distortion when subjected to an electric field of 500 MV/m along various directions, using self-consistent quantum molecular dynamics. In real materials, nanothreads or PVDF chains may be anchored at structural defects such as cross-links and grain boundaries. To establish a well-defined system for investigating the electromechanical response of mechanically pinned polar polymers, we anchored the two terminal formula units (C_4H_4O or $-CH_2-CF_2-$) at either end of nanothread or PVDF oligomers during MD simulations. In experimental settings one could employ angular optical tweezers[30] if a similar anchoring geometry was desired; here we utilize this simplified geometry

https://doi.org/10.1021/acs.nanolett.4c01431
Nano Lett. 2024, 24, 9195−9201

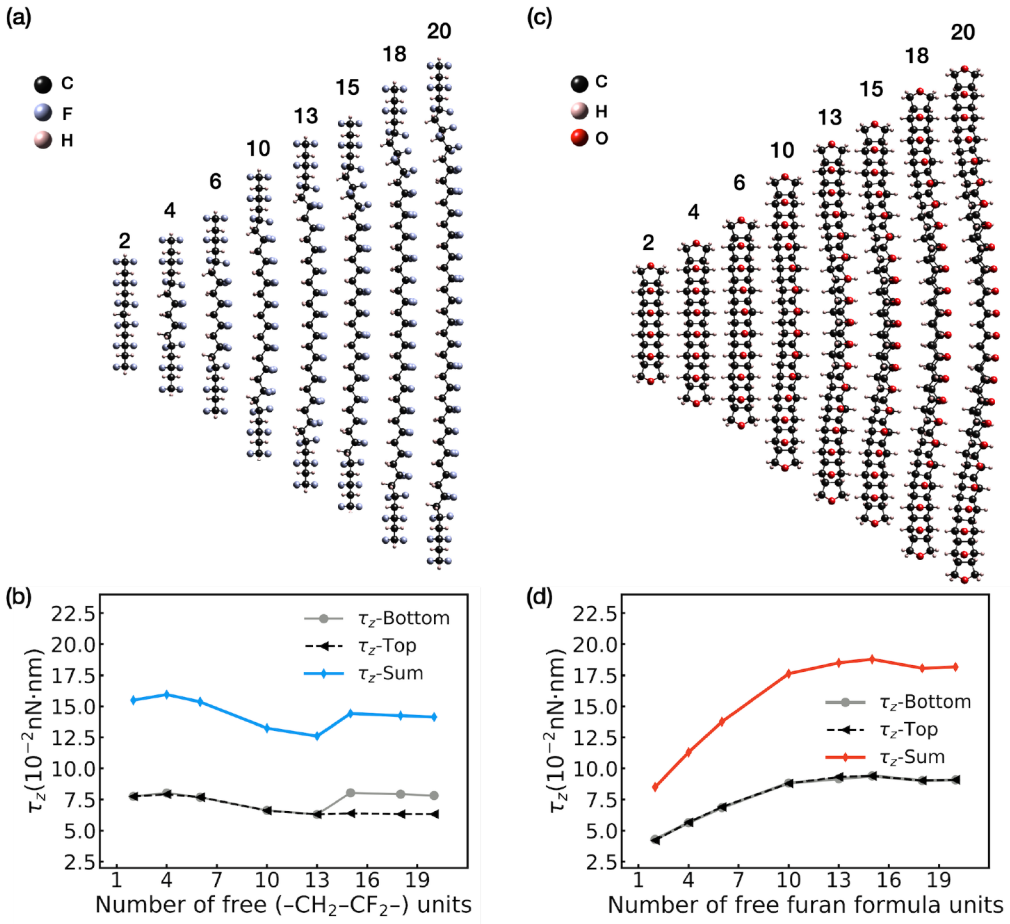

Figure 3. Twisting and bending of PVDF all-T and furan *syn* oligomers with an external electric field perpendicular to the chain axis. (a) Relaxed structures and (b) calculated torque along the chain axis from top and bottom fixed anchor atoms for PVDF all-T oligomers with different numbers of free (−CH_2−CF_2−) units. (c) Relaxed structures and (d) calculated torque along the chain axis from top and bottom fixed atoms for furan *syn* thread oligomers with different numbers of free furan formula units. The numerical labels in parts (a) and (c) are the number of free (−CH_2−CF_2−) units and furan formula units, respectively.

as a means to isolate and elucidate important aspects of single-chain response. A chain under these rigid constraints should behave similarly to a slightly shorter chain under more compliant mechanical constraints.

In the absence of electric field, the furan *syn* oligomer slightly bends away from the side with the oxygen atoms due to steric repulsion between oxygen atoms, while the CH_2 and CF_2 units of the PVDF all-T chain undergo significant distortion due to their mutual dipole interaction and the soft backbone of the chain, as shown in Figure S3. The net constraint force and torque on the oligomers summed over all atoms in both anchors are zero, as expected (Figure S4 and Figure S5).

When under a transverse field of 10 MV/m perpendicular to the dipole moment of the chain, the dipole moments of PVDF all-T oligomers aligned with the external electric field mainly through rotation about one σ bond near each anchor (i.e., a kink) with a uniform central region now aligned to the field, as shown in Figures 3a and S6. Because the system is relaxed into mechanical equilibrium under each electric field value, the net torque and force on the oligomer remains zero, as does the summed force exerted by the anchors on the oligomer, since the oligomer has no net charge. The x and y components of the torques exerted by the anchors are also zero because the electric field is perpendicular to the axis of the oligomer (Figure S7). However, the z component of the constraint torque exerted by the anchors is nonzero, because it balances the torque exerted by the electric field on the oligomer dipole. For PVDF, this torque is essentially independent of oligomer length (Figure 3b), since it is defined by the torque necessary to create a kink. Any further external field rotation simply swivels the kink, similar to the behavior of a constant-torque rotary spring. Thus, this system has minimal memory of its prior electric field history, nor does its response vary as a function of the length of the oligomer.

In sharp contrast, Figures 3c,d and S6 show how the furan oligomer under the field forms two opposing helices originating from the anchors; these helices create progressively larger torques for longer oligomers until the oligomer is so long that its central region aligns directly to the field. The net torques along x and y remain zero, while that along z reaches 18.4×10^{-2} nN·nm; higher values would be expected for threads with similar dipole moments per unit length but stiffer backbones. For orientation, this torque is an order of magnitude larger than that of a chromatin fiber ($\sim 10^{-2}$ nN·nm) twisted by angular optical tweezers.[30] The stark difference between PVDF and the polar nanothread arises from the torsional stiffness of the nanothread. The anchored thread resists alignment to the external field, and every dipolar subunit that is not well-aligned to the field (i.e., those within the helical sections) feels a nonzero torque from this field. The thread also

https://doi.org/10.1021/acs.nanolett.4c01431
Nano Lett. 2024, 24, 9195−9201

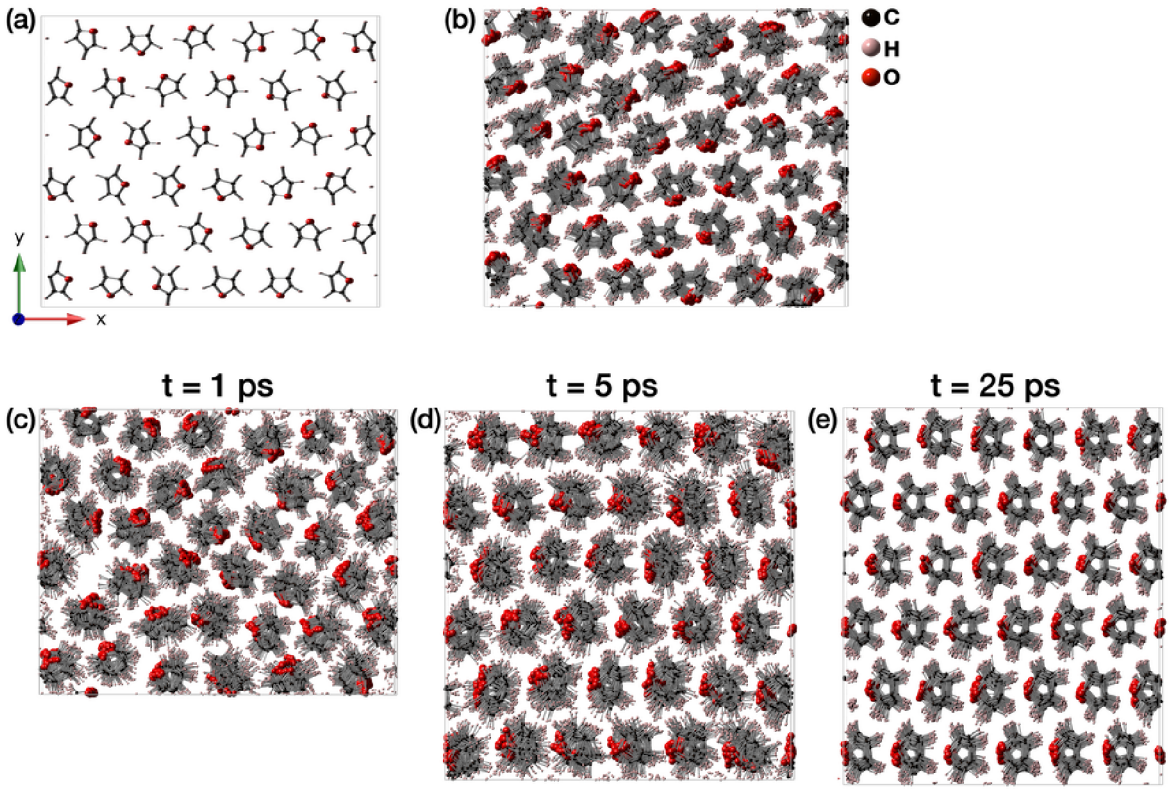

Figure 4. Poling of randomly packed furan *syn* threads was carried out by external electric fields at 300 K. (a) Randomly packed furan *syn* threads after energy minimization. (b) The equilibrium state of randomly packed furan *syn* threads without external electric field at 300 K. Poling of furan *syn* threads with electric field of 3 GV/m perpendicular to the thread axis at simulation times of (c) 1 ps, (d) 5 ps, and (e) 25 ps.

experiences an ever-increasing tensile strain as it twists (Figure S8), an effect absent in anchored PVDF because PVDF's field alignment is essentially entirely captured in a single kink.

The torsional stiffness of the thread backbone thus creates opportunities for new electromechanical couplings. The anchored nanothread develops tensile stress when twisted by a rotating electric field; under different boundary conditions (such as interthread cross-links), this would produce an axial shortening. The field-induced helical distortion should modulate other properties such as electrical conductivity or catalytic activity (by changing the overlap between successive oxygen p_z orbitals or other functionalities). Field coupling could be increased by attaching charged functionalities, and the maximal torque generated could be increased by using a polyaromatic precursor with a stiffer backbone. Twisting of thread samples anchored by cross-links could also enable significant mechanical energy storage.[31]

Poling of Bulk Samples by External Electric Fields. Prior investigations primarily focused on poling the crystalline α phase of PVDF.[26,32] However, the morphology of as-grown PVDF typically consists of spherulites with multiple α phase lamellar domains oriented diversely, introducing disorder in axial and azimuthal alignments between adjacent chains.[33] The experimental X-ray diffraction of furan nanothreads broadens upon release of pressure, possibly due to on-thread structural defects disrupting interthread alignment.[17,18] We thus examine the role of disorder through simulations of densely packed nanothread and PVDF samples starting from a random distribution of azimuthal orientations and axial shifts (Figure S9). In contrast to the poling of PVDF, which should proceed through rotations of CH_2 and CF_2 segments about σ bonds (see below), the poling of more rigid *syn* furan threads should occur through a more coherent backbone rotation. After energy minimization and equilibration at 300 K (Figure 4a, b), an initially random distribution of *syn* furan nanothread orientations and axial shifts is maintained in a simulation cell holding 60 furan repeats axially; this initial relaxation and equilibration serve to remove any especially high-energy local configurations that may have been introduced by the randomization of thread packing. This system is then subject (at 300 K) to external fields stepping from 2 to 10 GV/m in 1 GV/m increments until poling is achieved. The supercell is fully poled by an external electric field of 3 GV/m; smaller fields produce incomplete transient poling (i.e., a paraelectric response) over simulation time scales. Threads initially misaligned with the external electric field twist and untwist their backbones during poling (the untwisting being necessitated by periodic boundary conditions; Figure 4c). This suggests the excitation of softened torsional modes coupled to the external electric field. Those modes vanish as the threads achieve a field-aligned equilibrium state, as shown in Figure 4d,e. Concurrently, the initially random axial shifts transform into more homogeneous axial packing. The fully poled furan threads transform from an initially pseudohexagonal packing to a more densely packed tetragonal lattice, with the supercell parameters a shrinking substantially from 32.46 to 26.65 Å while b expands from 26.74 to 31.79 Å (Figure 4e). This large change in cell dimensions reflects a strong electromechanical coupling in the solid state, one that should coexist with the helicity-based coupling of anchored threads in samples whose thread orientations are pinned by a low linear density of pinning sites.

https://doi.org/10.1021/acs.nanolett.4c01431
Nano Lett. 2024, 24, 9195−9201

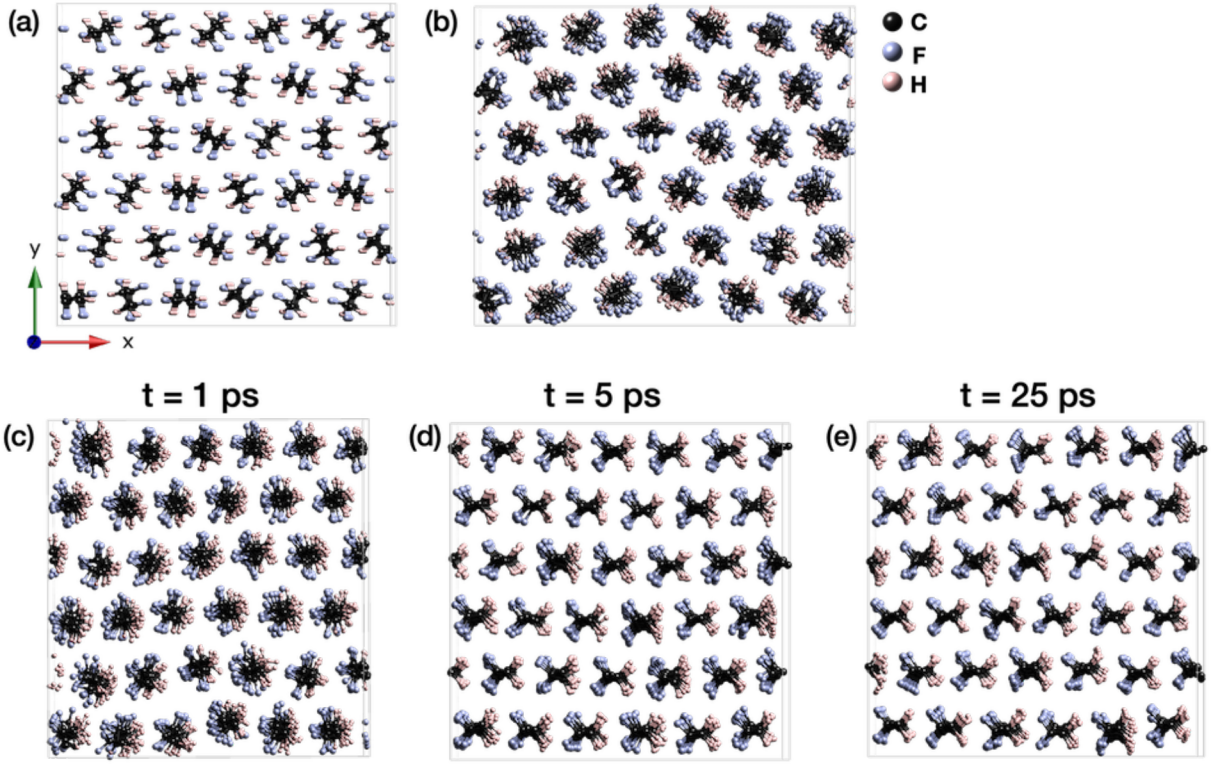

Figure 5. Poling of randomly packed PVDF TGTG′ chains by external electric fields at 50 K. (a) Randomly packed PVDF chains after energy minimization. (b) The equilibrium state of randomly packed PVDF chains without external electric field at 50 K. Poling of PVDF with electric field of 6 GV/m perpendicular to the chain axis at simulation times of (c) 1 ps, (d) 5 ps, and (e) 25 ps.

After energy minimization (Figure 5a), the PVDF TGTG′ chains remain in a random distribution of azimuthal angles and axial shifts. To ensure an accurate simulation of equilibration and the poling process, we conducted the MD simulations at 50 K instead of room temperature. This choice prevents thermal disordering of the original TGTG′ chain configuration; such a disruption would otherwise impede crystallization within computationally accessible simulation times. Following MD equilibration at T = 50 K without an external field (Figure 5b), the chains maintain random azimuthal orientations and axial shifts, albeit the CH_2 and CF_2 segments deviate slightly from the ideal TGTG′ conformation. Upon applying an external electric field as in the nanothread case, we observe a 6 GV/m threshold for the external field to fully transform randomly packed PVDF TGTG′ chains to the crystalline β phase. The transition occurs in two stages. First, the chain converts from the TGTG′ to "semi-all-T" conformation (shown in Figure S10) while simultaneously aligning the dipole moment of each chain with the electric field (Figure 5c). Next, each chain transforms from the semi-all-T conformation to the all-T state (Figure 5d). In the semi-all-T conformation, the CH_2 and CF_2 segments reside on the opposite sides of the backbone, similar to the all-T conformation, but the alignment of H and F atoms is not as precise as in the all-T conformation.

The extent of initial misalignment between the chain's dipole moment and the external electric field determines its mode of transformation in the first stage. Chains with dipole moments originally aligned or antialigned with the external electric field transform to the semi-all-T conformation through rotations of CH_2 and CF_2 segments, with smaller rotation angles for aligned chains and larger angle changes for antialigned chains. When the chain dipole moments are roughly orthogonal to the electric field, we observe a combination of coherent chain rotation and segment-by-segment CF_2/CH_2 rotation during progression toward the semi-all-T conformation. In the second stage, the $-CH_2-$ and $-CF_2-$ units continue to rotate from semi-all-T to all-T while the chains shift axially from the random distribution to an ordered packing registry, underlining a role for the electric field in developing translational order. Eventually the randomly packed PVDF TGTG′ chains are poled to the β phase with a preferential distribution of dipole moments toward the direction of the applied electric field, as shown in Figure 5e.

The two-stage transformation we observe shares similarities with the one proposed by Ranjan et al.,[32] with one notable distinction: in their initial stage, one of the TGTG′ chains within the unit cell of the α phase undergoes a 180-degree rotation, leading to the formation of the γ phase (i.e., two parallel TGTG′ chains within the unit cell) rather than the semi-all-T phase. Subsequently, both chains collectively alter their dihedral angles from ±57° to 180° to form the β phase. A reduced electric field can partially pole the packed chains, perhaps due to a weak chain−chain orientational interaction. These findings underscore the importance of the degree of order in the unpoled state when designing and optimizing experiments for achieving the desired phase transition.

The field thresholds required to induce these poling transitions in MD are significantly larger than those observed experimentally for PVDF (~100 MV/m.[29,34]). Simulations of the α-to-β phase transition using ReaxFF or Condensed-phase Optimized Molecular Potentials for Atomistic Simulation Studies (COMPASS)[35] also found a poling threshold of 5−10 GV/m.[26,36] The voltage to induce the PVDF $\alpha \rightarrow \beta$ phase

https://doi.org/10.1021/acs.nanolett.4c01431
Nano Lett. 2024, 24, 9195−9201

transition is higher than the experimental DC breakdown voltage (approximately 720−770 MV/m).[37] This discrepancy originates from the short time scale accessible to atomistic molecular dynamics and the absence of nucleation centers in the simulation, which is much smaller than the experimental sample. Thus, simulations of poling fields by these methods should be considered as upper bounds and means of establishing trends or comparisons, not as absolute quantitative predictions of experiments that take place on much longer time scales. Increasing temperature[38] or mechanical stretching[26,39] can facilitate the phase transition. In our simulations of furan nanothreads, the poling threshold decreases from 4 to 3 GV/m as the temperature increases from 50 to 300 K. The similarity of the simulated poling thresholds in PVDF (which is straightforward to pole experimentally) and *syn* furan nanothreads suggests that the poling of *syn* nanothreads may be similarly achievable. Keep in mind that the threads in this supercell are not cross-linked and thus are unanchored; for an experimental sample with some density of interthread cross-links one would anticipate a combination of the anchored and free behaviors described above, depending on the density of cross-links. Upon removal of the applied electric field, both PVDF and furan nanothread materials maintain their polarized states (see Figure S11) with modest changes in lattice constants (up ∼0.4% along *x* and down ∼0.7% and ∼0.04% along *y* and *z* for the nanothread; up ∼10.3% along *x* and down ∼1.7% and ∼0.6% along *y* and *z* for PVDF).

Since they originate from the generic properties of polarity and backbone rigidity, the general phenomena outlined here for *syn* furan-derived nanothreads should generalize to other species of nanothreads formed from polar precursors. The electromechanical coupling between axial length, axial tension, and rotational field history observed here for an anchored threads can likely be obtained in the solid state for cross-linked threads; this is a topic for future investigation. Such couplings open up new potential avenues for functional nanomaterials whose properties could be tuned through the introduction of polar or charged groups, changes of backbone stiffness, interthread couplings, and pinning at structural inhomogeneities.

■ ASSOCIATED CONTENT

Supporting Information

The Supporting Information is available free of charge at https://pubs.acs.org/doi/10.1021/acs.nanolett.4c01431.

ReaxFF$_{furan2024}$ reactive force field; DFT and MD simulations details; atomic charges for furan *syn* thread; crystalline structures for PVDF; relative energies for furan dimer and its transition state; structures of furan *syn* oligomer and PVDF all-T oligomer; calculated forces and torques in *x*, *y*, and *z* for PVDF all-T and furan *syn* oligomers; geometries for randomly packed and poled furan *syn* threads and PVDF; a semi-all-T conformation of PVDF chain. (PDF)th

ReaxFF reactive force field parameters for C/H/O/F/Al interactions (ReaxFF$_{PVDF}$) (TXT)

ReaxFF reactive force field parameters for furan nanothreads (ReaxFF$_{furan2024}$) (TXT)

■ AUTHOR INFORMATION

Corresponding Author

Adri C. T. van Duin − *Department of Mechanical Engineering, Pennsylvania State University, University Park, Pennsylvania 16802, United States; Department of Chemistry, Department of Materials Science and Engineering, and Department of Chemical Engineering, Pennsylvania State University, University Park, Pennsylvania 16802, United States;* orcid.org/0000-0002-3478-4945; Email: acv13@psu.edu

Authors

Tao Wang − *Department of Mechanical Engineering, Pennsylvania State University, University Park, Pennsylvania 16802, United States;* orcid.org/0000-0003-2833-1592

Yawei Gao − *Department of Mechanical Engineering, Pennsylvania State University, University Park, Pennsylvania 16802, United States*

Bo Chen − *Donostia International Physics Center, 20018 Donostia, San Sebastián, Spain; IKERBASQUE, Basque Foundation for Science, 48009 Bilbao, Spain;* orcid.org/0000-0002-5084-1321

Vincent H. Crespi − *Department of Chemistry, Department of Physics, and Department of Materials Science and Engineering, Pennsylvania State University, University Park, Pennsylvania 16802, United States*

Complete contact information is available at: https://pubs.acs.org/10.1021/acs.nanolett.4c01431

Notes

The authors declare no competing financial interest.

■ ACKNOWLEDGMENTS

This work is supported by the AFOSR MURI contract no. FA9550-19-1-0008. B.C. acknowledges the financial support from MCIN/AEI/10.13039/501100011033/FEDER, UE (project PID2021-123573NA-I00). T.W. and V.H.C. acknowledge additional support from the National Science Foundation under DMR-2011839.

■ REFERENCES

(1) Fitzgibbons, T. C.; Guthrie, M.; Xu, E.; Crespi, V. H.; Davidowski, S. K.; Cody, G. D.; Alem, N.; Badding, J. V. Benzene-Derived Carbon Nanothreads. *Nat. Mater.* **2015**, *14* (1), 43−47.

(2) Li, X.; Baldini, M.; Wang, T.; Chen, B.; Xu, E.; Vermilyea, B.; Crespi, V. H.; Hoffmann, R.; Molaison, J. J.; Tulk, C. A.; Guthrie, M.; Sinogeikin, S.; Badding, J. V. Mechanochemical Synthesis of Carbon Nanothread Single Crystals. *J. Am. Chem. Soc.* **2017**, *139* (45), 16343−16349.

(3) Duan, P.; Li, X.; Wang, T.; Chen, B.; Juhl, S. J.; Koeplinger, D.; Crespi, V. H.; Badding, J. V.; Schmidt-Rohr, K. The Chemical Structure of Carbon Nanothreads Analyzed by Advanced Solid-State NMR. *J. Am. Chem. Soc.* **2018**, *140* (24), 7658−7666.

(4) Wang, T.; Duan, P.; Xu, E.-S.; Vermilyea, B.; Chen, B.; Li, X.; Badding, J. V.; Schmidt-Rohr, K.; Crespi, V. H. Constraining Carbon Nanothread Structures by Experimental and Calculated Nuclear Magnetic Resonance Spectra. *Nano Lett.* **2018**, *18* (8), 4934−4942.

(5) Iijima, S. Helical Microtubules of Graphitic Carbon. *Nature* **1991**, *354* (6348), 56−58.

(6) Xu, E.; Lammert, P. E.; Crespi, V. H. Systematic Enumeration of Sp ^{3} Nanothreads. *Nano Lett.* **2015**, *15* (8), 5124−5130.

(7) Li, X.; Wang, T.; Duan, P.; Baldini, M.; Huang, H.-T.; Chen, B.; Juhl, S. J.; Koeplinger, D.; Crespi, V. H.; Schmidt-Rohr, K.; Hoffmann, R.; Alem, N.; Guthrie, M.; Zhang, X.; Badding, J. V.

Carbon Nitride Nanothread Crystals Derived from Pyridine. *J. Am. Chem. Soc.* **2018**, *140* (15), 4969−4972.
(8) Biswas, A.; Ward, M. D.; Wang, T.; Zhu, L.; Huang, H.-T.; Badding, J. V.; Crespi, V. H.; Strobel, T. A. Evidence for Orientational Order in Nanothreads Derived from Thiophene. *J. Phys. Chem. Lett.* **2019**, *10* (22), 7164−7171.
(9) Huang, H.-T.; Zhu, L.; Ward, M. D.; Wang, T.; Chen, B.; Chaloux, B. L.; Wang, Q.; Biswas, A.; Gray, J. L.; Kuei, B.; Cody, G. D.; Epshteyn, A.; Crespi, V. H.; Badding, J. V.; Strobel, T. A. Nanoarchitecture through Strained Molecules: Cubane-Derived Scaffolds and the Smallest Carbon Nanothreads. *J. Am. Chem. Soc.* **2020**, *142* (42), 17944−17955.
(10) Ward, M. D.; Tang, W. S.; Zhu, L.; Popov, D.; Cody, G. D.; Strobel, T. A. Controlled Single-Crystalline Polymerization of $C_{10}H_8 \cdot C_{10}F_8$ under Pressure. *Macromolecules* **2019**, *52* (20), 7557−7563.
(11) Gerthoffer, M. C.; Wu, S.; Chen, B.; Wang, T.; Huss, S.; Oburn, S. M.; Crespi, V. H.; Badding, J. V.; Elacqua, E. 'Sacrificial' Supramolecular Assembly and Pressure-Induced Polymerization: Toward Sequence-Defined Functionalized Nanothreads. *Chem. Sci.* **2020**, *11* (42), 11419−11424.
(12) Gerthoffer, M. C.; Xu, B.; Wu, S.; Cox, J.; Huss, S.; Oburn, S. M.; Lopez, S. A.; Crespi, V. H.; Badding, J. V.; Elacqua, E. Mechanistic Insights into the Pressure-Induced Polymerization of Aryl/Perfluoroaryl Co-Crystals. *Polym. Chem.* **2022**, *13* (10), 1359−1368.
(13) Tang, W. S.; Strobel, T. A. Evidence for Functionalized Carbon Nanothreads from π-Stacked, Para-Disubstituted Benzenes. *J. Phys. Chem. C* **2020**, *124* (45), 25062−25070.
(14) Romi, S.; Fanetti, S.; Alabarse, F.; Mio, A. M.; Bini, R. Synthesis of Double Core Chromophore-Functionalized Nanothreads by Compressing Azobenzene in a Diamond Anvil Cell. *Chem. Sci.* **2021**, *12* (20), 7048−7057.
(15) Romi, S.; Fanetti, S.; Alabarse, F.; Mio, A. M.; Haines, J.; Bini, R. Towards Custom Built Double Core Carbon Nanothreads Using Stilbene and Pseudo-Stilbene Type Systems. *Nanoscale* **2022**, *14* (12), 4614−4625.
(16) Gao, D.; Tang, X.; Xu, J.; Yang, X.; Zhang, P.; Che, G.; Wang, Y.; Chen, Y.; Gao, X.; Dong, X.; Zheng, H.; Li, K.; Mao, H. Crystalline $C_3N_3H_3$ Tube (3,0) Nanothreads. *Proc. Natl. Acad. Sci. U. S. A.* **2022**, *119* (17), No. e2201165119.
(17) Huss, S.; Wu, S.; Chen, B.; Wang, T.; Gerthoffer, M. C.; Ryan, D. J.; Smith, S. E.; Crespi, V. H.; Badding, J. V.; Elacqua, E. Scalable Synthesis of Crystalline One-Dimensional Carbon Nanothreads through Modest-Pressure Polymerization of Furan. *ACS Nano* **2021**, *15* (3), 4134−4143.
(18) Matsuura, B. S.; Huss, S.; Zheng, Z.; Yuan, S.; Wang, T.; Chen, B.; Badding, J. V.; Trauner, D.; Elacqua, E.; van Duin, A. C. T.; Crespi, V. H.; Schmidt-Rohr, K. Perfect and Defective ^{13}C-Furan-Derived Nanothreads from Modest-Pressure Synthesis Analyzed by ^{13}C NMR. *J. Am. Chem. Soc.* **2021**, *143* (25), 9529−9542.
(19) Chen, B.; Crespi, V. H.; Hoffmann, R. Theoretical Studies of Furan and Thiophene Nanothreads: Structures, Cycloaddition Barriers, and Activation Volumes. *J. Am. Chem. Soc.* **2022**, *144* (20), 9044−9056.
(20) Wang, X.; Yang, X.; Wang, Y.; Tang, X.; Zheng, H.; Zhang, P.; Gao, D.; Che, G.; Wang, Z.; Guan, A.; Xiang, J.-F.; Tang, M.; Dong, X.; Li, K.; Mao, H. From Biomass to Functional Crystalline Diamond Nanothread: Pressure-Induced Polymerization of 2,5-Furandicarboxylic Acid. *J. Am. Chem. Soc.* **2022**, *144* (48), 21837−21842.
(21) Dunning, S. G.; Chen, B.; Zhu, L.; Cody, G. D.; Chariton, S.; Prakapenka, V. B.; Zhang, D.; Strobel, T. A. Synthesis and Post-Processing of Chemically Homogeneous Nanothreads from 2,5-Furandicarboxylic Acid**. *Angew. Chem., Int. Ed.* **2023**, *62* (14), No. e202217023.
(22) Reynoso, A.; Xu, B.; Crespi, V. H. Controlling Nanothread Backbone Structure through Precursor Design. arXiv February 15, 2023. DOI: 10.48550/arXiv.2302.07482.
(23) Ruan, L.; Yao, X.; Chang, Y.; Zhou, L.; Qin, G.; Zhang, X. Properties and Applications of the β Phase Poly(Vinylidene Fluoride). *Polymers* **2018**, *10* (3), 228.
(24) Bohlén, M.; Bolton, K. Inducing the β-Phase of Poly-(Vinylidene Fluoride) : A Review. *Annu. Rev. Nanosci. Nanotechnol.* **2014**, *1* (1), No. 150110.
(25) Chenoweth, K.; van Duin, A. C. T.; Goddard, W. A. ReaxFF Reactive Force Field for Molecular Dynamics Simulations of Hydrocarbon Oxidation. *J. Phys. Chem. A* **2008**, *112* (5), 1040−1053.
(26) Gao, Y.; Zhu, W.; Wang, T.; Yilmaz, D. E.; van Duin, A. C. T. C/H/O/F/Al ReaxFF Force Field Development and Application to Study the Condensed-Phase Poly(Vinylidene Fluoride) and Reaction Mechanisms with Aluminum. *J. Phys. Chem. C* **2022**, *126* (27), 11058−11074.
(27) Swope, W. C.; Andersen, H. C.; Berens, P. H.; Wilson, K. R. A Computer Simulation Method for the Calculation of Equilibrium Constants for the Formation of Physical Clusters of Molecules: Application to Small Water Clusters. *J. Chem. Phys.* **1982**, *76* (1), 637−649.
(28) Thompson, A. P.; Aktulga, H. M.; Berger, R.; Bolintineanu, D. S.; Brown, W. M.; Crozier, P. S.; in 't Veld, P. J.; Kohlmeyer, A.; Moore, S. G.; Nguyen, T. D.; Shan, R.; Stevens, M. J.; Tranchida, J.; Trott, C.; Plimpton, S. J. LAMMPS - a Flexible Simulation Tool for Particle-Based Materials Modeling at the Atomic, Meso, and Continuum Scales. *Comput. Phys. Commun.* **2022**, *271*, No. 108171.
(29) Ramos, M. M. D.; Correia, H. M. G.; Lanceros-Méndez, S. Atomistic Modelling of Processes Involved in Poling of PVDF. *Comput. Mater. Sci.* **2005**, *33* (1), 230−236.
(30) Bustamante, C. J.; Chemla, Y. R.; Liu, S.; Wang, M. D. Optical Tweezers in Single-Molecule Biophysics. *Nat. Rev. Methods Primer* **2021**, *1* (1), 25.
(31) Zhan, H.; Zhang, G.; Bell, J. M.; Tan, V. B. C.; Gu, Y. High Density Mechanical Energy Storage with Carbon Nanothread Bundle. *Nat. Commun.* **2020**, *11* (1), 1905.
(32) Ranjan, V.; Nardelli, M. B.; Bernholc, J. Electric Field Induced Phase Transitions in Polymers: A Novel Mechanism for High Speed Energy Storage. *Phys. Rev. Lett.* **2012**, *108* (8), No. 087802.
(33) Lovinger, A. J. Ferroelectric Polymers. *Science* **1983**, *220* (4602), 1115−1121.
(34) YE, Y.; JIANG, Y.; WU, Z.; ZENG, H. Phase Transitions of Poly(Vinylidene Fluoride) Under Electric Fields. *Integr. Ferroelectr.* **2006**, *80* (1), 245−251.
(35) Sun, H. COMPASS: An Ab Initio Force-Field Optimized for Condensed-Phase ApplicationsOverview with Details on Alkane and Benzene Compounds. *J. Phys. Chem. B* **1998**, *102* (38), 7338−7364.
(36) Chelakara Satyanarayana, K.; Bolton, K. Molecular Dynamics Simulations of α- to β-Poly(Vinylidene Fluoride) Phase Change by Stretching and Poling. *Polymer* **2012**, *53* (14), 2927−2934.
(37) Jow, T. R.; Cygan, P. J. Investigation of Dielectric Breakdown of Polyvinylidene Fluoride Using AC and DC Methods. In *Conference Record of the 1992 IEEE International Symposium on Electrical Insulation*; IEEE: Baltimore, MD, USA, 1992; pp 181−184. DOI: 10.1109/ELINSL.1992.247024.
(38) Gregorio, R., Jr.; CapitãO, R. C. Morphology and Phase Transition of High Melt Temperature Crystallized Poly(Vinylidene Fluoride). *J. Mater. Sci.* **2000**, *35* (2), 299−306.
(39) Li, L.; Zhang, M.; Rong, M.; Ruan, W. Studies on the Transformation Process of PVDF from α to β Phase by Stretching. *RSC Adv.* **2014**, *4* (8), 3938−3943.

https://doi.org/10.1021/acs.nanolett.4c01431
Nano Lett. 2024, 24, 9195−9201